Supporting Information

Catalysis Science & Technology's

Bridging the gap between academic and industrial hydrocracking: on catalyst and operating conditions effects

Pedro S. F. Mendes[a,b,1]*, João M. Silva[a,c], M. Filipa Ribeiro[a], , Antoine Daudin[b], Christophe Bouchy[b*]

[a]*Centro de Química Estrutural, Instituto Superior Técnico, Universidade de Lisboa, Av. Rovisco Pais, 1049-001 Lisboa, Portugal*

[b]*IFP Energies nouvelles, Rond-point de l'échangeur de Solaize, BP 3, 69360 Solaize, France*

[c]*ADEQ-ISEL, Instituto Superior de Engenharia de Lisboa, Instituto Politécnico de Lisboa, R. Cons. Emídio Navarro, 1959-007 Lisboa, Portugal*

*pedro.f.mendes@tecnico.ulisboa.pt; christophe.bouchy@ifpen.fr ; +33 (0)4 37 70 29 89

Contents

[1] Present address: Laboratory for Chemical Technology, Ghent University, B-9052 Ghent, Belgium.

SI.1 Catalytic testing procedures

n-Hexadecane hydroconversion in the absence of H_2S and NH_3

The hydroisomerization of pure *n*-hexadecane in high-pressure conditions took place in a *Catatest* catalytic test unit with a fixed-bed downflow reactor operated in gas-phase. The catalysts powder was shaped into 0.2-0.35 mm and diluted with SiC (1:7 mass ratio). The catalytic bed had a diameter of 15 mm and a height of 25 mm. The products were separated at room temperature and reaction pressure. The gas products were sampled using a glass ampoule with known volume. Cis-2-butene was used as an internal by systematic addition of fixed quantity of this gas to the ampoule. The gas products were then analysed in a GC-FID equipment with a CP-Sil 5CB capillary column. The liquid products recovered were weighed and analyzed in a GC-FID equipment with a HP PONA capillary column. The carbon balance closed with a maximal deviation of ±5 %, according to the comparison between the inlet flowrate of *n*-C_{16} and the flowrate and the composition of the outlet gas stream and the mass of the liquid outlet.

n-Hexadecane hydroconversion in presence of H_2S and NH_3

The hydroisomerization of *n*-hexadecane in presence of H_2S and NH_3 took place in two catalytic test units with fixed-bed downflow reactors operated in gas-phase. The units differed on the operating space velocities: 1-4 $g_{nC16}\ g_{catalyst}^{-1}\ h^{-1}$ for the "high-feed" unit and 0.2-1.0 $g_{nC16}\ g_{catalyst}^{-1}\ h^{-1}$ for the "low-feed" unit. H_2S was generated through decomposition of dimethyl disulphide in the feedstock and NH_3 through decomposition of aniline in the feedstock. Complete decomposition in the reactor was verified by the absence of both compounds in the outlet stream. The feed composition is detailed in Table SI1.

Table SI1: Feedstock composition for *n*-hexadecane hydroconversion in presence of NH_3 and H_2S.

Compound	Sulphidation	Reaction
***n*-Hexadecane (wt.%)**	93.5	98.0
Dimethyl disulphide (wt.%)	6.0	1.5
Aniline (wt.%)	0.50	0.50

In the "high-feed" unit, the catalytic bed had a diameter of 16 mm and a height of 100 mm. The products were separated into a gas and a liquid outlet by a system separators described elsewhere [1]. The gas products were analyzed on-line in a GC-FID equipment with a CP-Sil 5CB capillary column. The liquid products recovered were weighed and analyzed in a GC-FID equipment with a HP PONA capillary column. The material balance closed with a maximal deviation of ±5 %, according to the comparison between the inlet flowrate of *n*-C_{16} and the flowrate and the composition of the outlet gas stream and the mass of the liquid outlet. In the "low-feed" unit, the catalytic bed had a diameter of 10 mm and a height of 100 mm. The products were sampled on-line without separation by the means of Kämmer valve. The GC-FID was equipped with a HP-PONA capillary column. A reference catalyst was tested in both units showing a relative deviation between catalytic tests units below ±5% for conversion and ±2% for C_{16} isomers yield.

SI.2 *n*-Hexadecane hydroconversion in the absence of H_2S and NH_3 over Pt/HUSY

Table SI2: Catalytic activity and turnover frequency over protonic sites over Pt/HUSY catalyst.

Temperature (K)	Activity (μmol g^{-1} s^{-1})	TOF_{Al} x 10^3 (s^{-1})
528	13	16
538	28	34
548	61	75

SI.3 NiMoS/(HUSY+Al_2O_3) characterization

Experimental procedures

The electron probe micro analysis (EPMA) were carried out in a *JEOL JXA 8100* equipment. The detailed procedure can be found elsewhere [2]. Locally measured concentrations were then processed using the method of the distance transform [3] to obtain the overall concentration of each element in the extrudate. The distribution coefficient R_{element} was calculated as the ratio of the mean concentration along the extrudate to overall concentration assuming a spherical grain of diameter $2r$ equal to the length of the profile [4] (vide SI for details). By these means, a distribution coefficient close to 1 means a uniform distribution of the element along the extrudate diameter. Otherwise, the coefficient will be higher than 1, if the concentration is greater in the core than at the edges (so-called egg-yolk distribution); and lower than 1 if the concentration is greater at the edges than in the core (so-called egg-shell distribution) [4]. By measuring the local concentrations in silicon and aluminium, the concentration of nickel and molybdenum in the zeolite and the alumina could be determined [5, 6].

Results

In this section, the characterization for the three catalyst samples with different molybdenum loading is presented and briefly discussed altogether.

Elemental analysis via x-ray fluorescence confirmed the variation in the Mo loading in the catalysts while the nickel and phosphorous to molybdenum atomic ratios remained constant at ca. 0.40 and 0.48, respectively (Table SI3).

Table SI3: Composition of NiMo/(HUSY+Al_2O_3) samples targeted and as measured by XRF.

Sample	Targeted Mo content (wt.%)	Measured Mo content (wt.%)	Zeolite (wt.%)	Targeted Ni/Mo (atomic)	Measured Ni/Mo (atomic)	Targeted P/Mo (atomic)	Measured P/Mo (atomic)
9NiMo/(HUSY+Al_2O_3)	9	8.9	13.3	0.40	0.40	0.48	0.47
12NiMo/(HUSY+Al_2O_3)	13	12.0	11.9		0.40		0.49
16NiMo/(HUSY+Al_2O_3)	17	16.1	10.4		0.40		0.47

The micrometric distribution of these elements throughout the extrudates diameter was investigated via Electron Probe Micro Analysis (EPMA). For the calcined samples (designated “NiMo”), the distribution coefficient, defined as the ratio of the mean concentration along the extrudate to overall concentration (vide section 2.2 of the article), of Ni and Mo was 0.98 in average and no impact of Mo content was observed (Figure SI1a). Therefore, a uniform distribution of Ni and Mo along the extrudate diameter was achieved with this NiMo introduction procedure, as previously revealed as well [2]. For a selected sample (12NiMoS/(Al_2O_3+HUSY), the elemental distribution was assessed after *ex-situ* sulfidation. The distribution coefficient of sulfur was also very close to one (0.98) pointing to a homogeneous sulfidation throughout the extrudates diameter. After sulfidation both Ni and Mo remained well distributed in the extrudates as their distribution coefficients were equal to 0.96 and 0.98

respectively. These results further validated the catalyst preparation procedure previously established [2]. Furthermore, the elemental distribution in calcined samples seemed to be representative of that in sulfided (i.e. catalytic) samples.

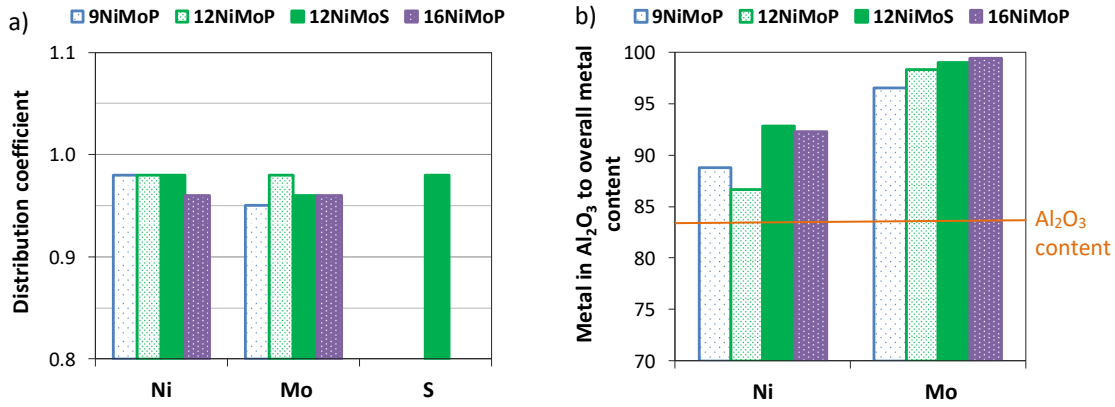

Figure SI1: a) Elemental distribution coefficient along the extrudates for nickel, molybdenum and sulfur. b) Fraction of nickel and molybdenum content deposed in the alumina for HUSY. The line corresponds to an even distribution of the metal between the zeolite and the alumina.

The concentration profiles of silicon was also measured, revealing a uniform distribution of zeolite in the alumina matrix (Table SI4), as previously observed as well for this support [5]. The quantification of both Al and Si enabled the identification of zeolite-rich (in presence of silicon) and alumina-rich (in absence of silicon) domains along the extrudates. The metal content in both the zeolite and the alumina was thus estimated. In Figure SI1b), the percentage of metal located in the alumina is plotted and compared to the percentage of alumina in the support. For both nickel and molybdenum, the content in alumina was larger than the fraction of alumina in the support. The metals were thus preferentially located in the alumina. Nevertheless, whereas the fraction of Mo in the alumina was always above 95%, that of Ni was 90% in average, closer to the fraction of alumina in the support (83.5%). Ni was thus present in both components of the support whereas Mo was practically absent from the zeolite.

Table SI4: Elemental distribution along the extrudates of NiMo/(HUSY+Al_2O_3) samples as measured by EPMA.

Sample	Distribution coefficient Ni	Distribution coefficient Mo	Distribution coefficient P	Distribution coefficient S	Distribution coefficient Si	Distribution coefficient Al
9NiMo/(HUSY+Al_2O_3)	1.01	0.98	0.91	-	1.03	1.03
12NiMo/(HUSY+Al_2O_3)	0.98	0.98	0.91	-	0.98	1.01
12NiMoS/(HUSY+Al_2O_3)	0.96	0.98	0.91	0.98	1.01	1.02
16NiMo/(HUSY+Al_2O_3)	0.96	0.96	0.94	-	1.02	1.02

The fact that molybdenum and nickel had not the same distribution between zeolite and alumina may lead to different promoted MoS_2 phases in each support. On the one hand, less than 5% of the molybdenum was placed in the zeolite. On the other hand, as the active phase is made up of Ni promoted MoS_2 sites [7], the higher Ni/Mo ratio observed in the zeolite might result in higher amount of NiMoS sites. Taking into account the average

values of Mo and Ni content in either zeolites or alumina, the average Ni/Mo (atomic) ratio was estimated in 2.4 and 0.44, respectively. According to literature, for a slab length of 3.3 nm (see Table SI5), the optimal Ni/Mo atomic ratio in the nanocrystallites of MoS_2 is 0.5 [7]. For Ni/Mo ratios higher than 0.5, further addition of nickel no longer results in the decoration of Mo atoms leading instead to the decoration of Ni atoms, forming thus NiS_x sites [7] which are much less active in hydrogenation reactions [8]. Additionally, the direct deposition of Ni on zeolites has been reported to lead to Ni^{2+} species in exchange positions of zeolites or NiO particles [9, 10]. In this case, such species might also be present then. Therefore, despite the suspected superior promotion level over zeolites, most of the additional nickel shall be under rather inactive forms, resulting in a minor fraction of NiMoS sites (at most 5%) located in the zeolite. In short, practically all the HDH function in NiMoS catalysts was located in the alumina.

The deposition of metals in solid supports depends on, among other parameters, the interaction between metal precursors and support. In impregnation aqueous solution, Mo is expected to be mainly in the form an Strandberg-type heteropolyanion ($P_2Mo_5O_{23}^{6-}$) because the P/Mo ratio in solution is similar to the stoichiometry of such HPAs which are also stable in acidic medium [11, 12]. Meanwhile, dissociation of $Ni(OH)_2$ should lead to a hydrated Ni^{2+} complex, as the interaction between Ni^{2+} and HPA is not so favored under these conditions [13]. In weak acidic medium (expected here due to the presence of H_3PO_4) the surface of alumina should be positively charged, contrarily to that of zeolites [2]. Thereby, the negatively charged molybdenum species will preferably interact with the alumina whereas Ni is expected to interact mainly with the zeolite. The higher fraction of Ni introduced in the zeolite compared to that of Mo seemed hence in agreement with the expected behavior in terms of metal-support interaction, even though dedicated experiments would be necessary to confirm this proposition.

The concentration of NiMoS sites (n_{NiMoS}) ranged from 0.19 to 0.34 mmol g^{-1} (Table SI5). It is worth mentioning that the atomic Ni/Mo ratio of the MoS_2 slabs was about 0.28 and so somewhat lower than the bulk Ni/Mo ratio (Table SI5). The average slab length (assessed by TEM) was also found to be independent of the Mo content, around ca. 3.3 nm (Table SI5). Based on NiMoS sites concentration, the amount of Mo incorporated in the NiMoS site could be assessed. It corresponded to ca. 15% of the overall Mo deposed on the catalyst. The corresponding NiMoS to Al^{IV} ratio ranged from 1.8 to 4.0 (Table SI5).

Table SI5: Composition of NiMoS/($HUSY+Al_2O_3$) samples as measured by XPS, slab length by TEM, /concentration of NiMoS sites, and HDH to acid sites ratio.

Sample	Mo content (wt.%)	MoS_2/ $Mo_{overall}$ (mol%)	NiMoS/ $Ni_{overall}$ (mol%)	$(Ni/Mo)_{slabs}$ (atomic)	$(Ni)MoS_2$ slab length (nm)	n_{NiMoS}/n_{Mo} (mol.%)	n_{NiMoS} sites (mmol g_{cat}^{-1})	n_{NiMoS}/n_{Al} (mol/mol)
9NiMoS/ ($HUSY+Al_2O_3$)	8.9	78	52	0.27	3.3	17	0.19	1.8
12NiMoS/ ($HUSY+Al_2O_3$)	12.0	69	55	0.30	3.2	16	0.28	2.9
16NiMoS/ ($HUSY+Al_2O_3$)	16.1	73	51	0.28	3.5	13	0.34	4.0

SI.4 *n*-Hexadecane hydroconversion in presence of H_2S and NH_3 NiMoS/(HUSY+Al_2O_3)

Figure SI2a) depicts the evolution of reactant conversion with the space velocity over zeolite at 633 K. The conversion of n-C_{16} decreased with increasing $WHSV_{zeolite}$, as expected. In Figure SI2b), the corresponding catalytic activity per mass of zeolite is plotted as function of the Mo loading. There was no noticeable evolution of the activity with Mo loading, even though the latter practically more than doubled the n_{NiMoS}/n_{Al} ratio. Assuming that the number of protonic sites was similar for all catalyst, this means that the turnover frequency remained constant over the range of HDH to acid sites ratio covered. This might indicate that the plateau of TOF_{Al} was reached [14, 15]. Mechanistically, this would mean that the dehydrogenation rate of the HDH function was sufficient to feed all the available Brønsted sites with intermediate olefins [14].

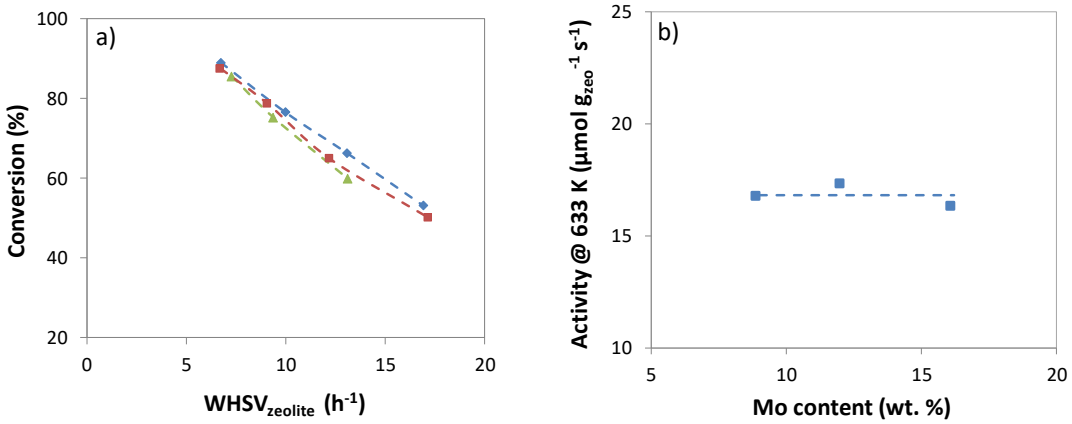

Figure SI2: a) *n*-Hexadecane conversion as function of weight space velocity over zeolite for a) NiMoS/(Al_2O_3+HUSY) catalysts at 633 K. Mo contents of 9% (■), 12% (◆), and 16% (▲). b) Catalytic activity per mass of zeolite for NiMoS/(Al_2O_3+HUSY). Symbols stand for experimental data and dashed lines for the mean of activities.

The yield of C_{16} isomers is represented as function of conversion in Figure SI3a). The range of conversions covered proved to be adequate, as the maximum isomer yield, the most sensitive selectivity indicator, could be identified. Differences between NiMoS/(Al_2O_3+HUSY) catalysts were slight but noticeable. With the purpose of analyzing the influence of molybdenum content, the maximal C_{16} isomer yield ($Y_{i\text{-}C16,max}$) at 633 K was plotted (Figure SI3b). $Y_{i\text{-}C16,max}$ increased slightly from 9 to 12 wt.% of molybdenum, seemingly reaching a plateau for Mo contents higher than 12 wt%. For well-balanced catalysts, i.e. whenever the HDH function is strong enough to feed all acid sites with olefins as well as to hydrogenate rapidly enough the *i*-olefins formed [14], a plateau of $Y_{i\text{-}C16,max}$ is to be expected. On the other hand, the range of n_{NiMoS}/n_{Al} ratio covered was relatively narrow: it only doubled with the increase in Mo content (Table SI5), whereas, when studying Pt/HUSY, n_{Pt}/n_{Al} increased by 9-fold [15]. Therefore, the minor evolution of maximal C_{16} isomers yield might also have been due to the narrow range of hydrogenating activities at stake. In fact, the observed improvement in the balance of acid function by HDH function with temperature (section 4.2 of the article) implied that catalysts were far from optimal balance at these operating conditions (i.e. high temperatures). Hence, the insensitivity of the catalytic performance to

increased molybdenum loadings pointed towards a relatively constant the metal-acid balance regardless of the Mo loading.

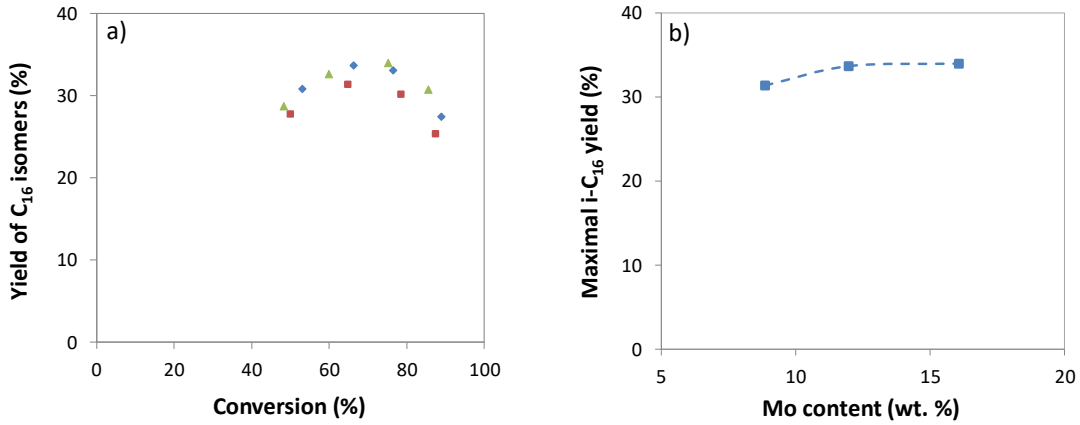

Figure SI3: a) Yield of C_{16} isomers as function of conversion for NiMoS/(Al_2O_3+HUSY) catalysts at 633 K. Mo contents of 9% (■), 12% (◆), and 16% (▲). b) Maximal yield of C_{16} isomers as a function of Mo content in the NiMoS/(Al_2O_3+HUSY) catalysts at 633 K.

SI.5 Estimation of vacant Brønsted acid sites

The methodology applied herein was developed in a previous work [2]. As ammonia is strongly adsorbed on the Brønsted sites of zeolites, one may assume that the adsorption of NH_3 is at the equilibrium. Moreover, as alkenes are much weaker bases, competition between the alkene intermediates and NH_3 is rather unlikely. In such conditions, the fraction of non-inhibited Brønsted sites (ψ_v) is only a function of temperature and NH_3 pressure. The data was collected for cyclohexane hydroconversion, over the same NiMoS/(Al_2O_3+HUSY) catalysts (12 and 16%, Mo loading) as in this study and under comparable operating conditions. The fraction of vacant Brønsted sites as a function of given partial pressure of NH_3 and temperature was estimated by the ratio of the activity at that pressure of NH_3 to the activity in absence of NH_3 at that same temperature [2]. Then, the Arrhenius equation was employed to obtain the kinetic parameters as a function of temperature.

The concentration of vacant acid sites (n_{Al}^{vacant}) at the operating temperatures and NH_3 partial pressure was herein estimated via the fraction of vacant sites at that temperature and pressure, employing the previously obtained parameters, times the overall concentration of sites (i.e. n_{Al}) – Eq. (SI.1).

$$n_{Al}^{vacant}\left(T, P_{NH_3}\right) = \psi_V\left(T, P_{NH_3}\right) \times n_{Al} \qquad \text{Equation (SI.1)}$$

SI.6 Cracking products

The overcracking index reflects the degree of secondary cracking exerted by a catalyst. If only pure primary cracking exists, the overcracking index will be 2 (molecules formed per C_{16} molecule cracked). Contrarily, if half of the cracked products undergo a second cracking step, the overcracking index will be 3 (molecules formed per C_{16} molecule cracked). In Figure SI4, 12NiMoS/(HUSY+Al_2O_3) revealed higher overcracking indexes comparatively to Pt/HUSY. Therefore, more consecutive cracking steps took place over the former, in agreement with the higher cracking rates for modes C and D at the tested temperatures, as discussed above.

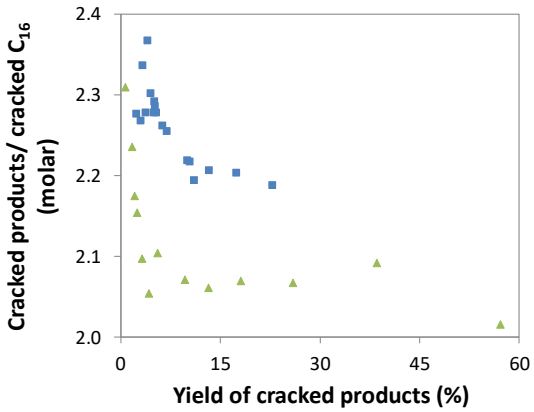

Figure SI4: Overcracking index as function of the cracked products yield over Pt/HUSY (▲) and 12NiMoS/(Al_2O_3+HUSY) catalyst (■) at 528-548 and 593-598 K, respectively.

As C_{16} isomers yield was similar when 12NiMoS/(HUSY+Al_2O_3) was tested at 593 and 598 K, the experimental data herein corresponds to those temperatures. In Figure SI5, the evolution of isomerization degree of cracked products is depicted as function of the yield of cracked products for Pt/HUSY and 12NiMoS/(HUSY+Al_2O_3) catalysts. In all cases, the isomerization degree increased along with the yield of cracked products in agreement with increasing MTB formation (and hence cracking) with conversion. The isomerization degree of the cracked products was clearly greater over Pt/HUSY than over 12NiMoS/(HUSY+Al_2O_3) catalysts, which can be explained by two phenomena. Firstly, every cracking reaction implies the loss of a branching degree. Additionally, the β-scission pathways have dissimilar activation energies. In hydrocracking at mild temperatures, β-scission mechanisms of type A and type B are preponderant, because only secondary and tertiary are involved [16-18]. On the other hand, this implies also that the activation energy of these cracking modes are lower than that of type C and type D [19]. Therefore, as the temperature increases, the cracking modes leading to less isomerized products become increasingly relevant, decreasing thus the isomerization degree in cracked products.

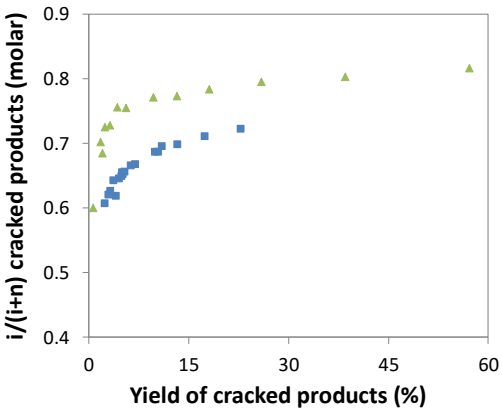

Figure SI5: Isomerization degree of cracked products as function of the cracked products yield over Pt/HUSY (▲) and 12NiMoS/(Al_2O_3+HUSY) catalyst (■). 12NiMoS/(HUSY+Al_2O_3) data correspond to 593 and 598 K. The isomerization degree was defined as the average content of isomerized products among all cracked products.

SI.7 References

1. J. Francis, PhD thesis, Université Claude Bernard Lyon 1, 2012.

2. P. S. F. Mendes, J. M. Silva, M. F. Ribeiro, C. Bouchy and A. Daudin, *Journal of Industrial and Engineering Chemistry*, 2019, **71**, 167-176.

3. L. Sorbier, F. Bazer-Bachi, Y. Blouet, M. Moreaud and V. Moizan-Basle, *Microscopy and Microanalysis*, 2016, **22**, 422–431.

4. L. Sorbier, in *Catalysis by Transition Metal Sulphides*, eds. H. Toulhoat and P. Raybaud, Ed. Technip, Paris, 2013, pp. 407–411.

5. P. S. F. Mendes, J. M. Silva, M. F. Ribeiro, A. Daudin and C. Bouchy, *Journal of Industrial and Engineering Chemistry*, 2018, **62**, 72-83.

6. S. Kasztelan, N. Marchal-George, T. Cseri, P. Leyrit, P. Dascotte and E. Rosenberg, *US 6531051*, 2003.

7. C. Legens and P. Raybaud, in *Catalysis by Transition Metal Sulphides*, eds. H. Toulhoat and P. Raybaud, Ed. Technip, Paris, 2013, pp. 259–300.

8. H. Toulhoat and P. Raybaud, in *Catalysis by Transition Metal Sulphides*, eds. H. Toulhoat and P. Raybaud, Ed. Technip, Paris, 2013, pp. 3–23.

9. J. Francis, E. Guillon, N. Bats, C. Pichon, A. Corma and L. J. Simon, *Applied Catalysis a-General*, 2011, **409**, 140–147.

10. I. Graça, L. V. González, M. C. Bacariza, A. Fernandes, C. Henriques, J. M. Lopes and M. F. Ribeiro, *Applied Catalysis B: Environmental*, 2014, **147**, 101–110.

11. C. Lamonier and E. Payen, in *Catalysis by Transition Metal Sulphides*, eds. H. Toulhoat and P. Raybaud, Ed. Technip, Paris, 2013, pp. 151–181.

12. B. Hedman, *Acta Crystallographica Section B Structural Crystallography and Crystal Chemistry*, 1977, **33**, 3083–3090.

13. A. Griboval, PhD thesis, Université de Lille, 1998.

14. F. Alvarez, F. R. Ribeiro, G. Perot, C. Thomazeau and M. Guisnet, *Journal of Catalysis*, 1996, **162**, 179–189.

15. P. S. F. Mendes, J. M. Silva, M. F. Ribeiro, P. Duchêne, A. Daudin and C. Bouchy, *AIChE Journal*, 2017, **63**, 2864-2875.

16. J. A. Martens, P. A. Jacobs and J. Weitkamp, *Applied Catalysis*, 1986, **20**, 239–281.

17. J. A. Martens, P. A. Jacobs and J. Weitkamp, *Applied Catalysis*, 1986, **20**, 283–303.

18. J. Weitkamp, *Chemcatchem*, 2012, **4**, 292–306.

19. J. W. Thybaut, C. S. L. Narasimhan, J. F. Denayer, G. V. Baron, P. A. Jacobs, J. A. Martens and G. B. Marin, *Industrial & Engineering Chemistry Research*, 2005, **44**, 5159–5169.